Resources, Conservation & Recycling 188 (2023) 106718

Contents lists available at ScienceDirect

Resources, Conservation & Recycling

journal homepage: www.elsevier.com/locate/resconrec

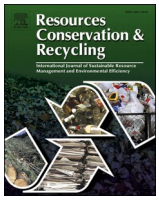

Full length article

# Deep learning for chemometric analysis of plastic spectral data from infrared and Raman databases

Edward Ren Kai Neo [a,b,*], Jonathan Sze Choong Low [b], Vannessa Goodship [a], Kurt Debattista [a]

[a] Warwick Manufacturing Group, University of Warwick, Coventry, CV4 7AL, United Kingdom
[b] Singapore Institute of Manufacturing Technology, 2 Fusionopolis Way, Singapore 138634, Singapore

ARTICLE INFO

*Keywords:*
Chemometrics
Spectroscopy
Deep learning
CNN
Plastic recycling
Automatic sorting

ABSTRACT

Increasing plastic recycling rates is key to addressing plastic pollution. New technologies such as chemometric analysis of spectral data have shown great promises in improving the plastic sorting efficiency to boost recycling rates. In this work, a novel deep learning architecture, PolymerSpectraDecisionNet (PSDN) was developed, consisting of convolutional neural networks, residual networks and inception networks in a decision tree structure. To better represent the conditions in the plastic recycling industry, the models were built to identify the most widely recycled polymers – polyethylene, polypropylene and polyethylene terephthalate from open-sourced infrared and Raman spectral dataset containing over 20 different polymers. PSDN performed better than end-to-end neural networks, obtaining an accuracy of 0.949 and 0.967 with the Raman and infrared datasets respectively. The use of deep learning can also distinguish between weathered and unaged polymer samples, with accuracies of 0.954 for high density polyethylene and 0.906 for polyethylene terephthalate.

## 1. Introduction

Plastic is an indispensable part of the world today, widely used in various industries such as packaging, construction, medical and agriculture. In 2020, global plastic production topped up at 368 million tons (Plastics Europe, 2022), representing a 200-fold increase over the past 70 years (Geyer et al., 2017; Ritchie, 2018). A significant percentage of plastic ever produced were landfilled, while only 9% has been recycled (Geyer et al., 2017). Mismanagement of plastic waste is a global environmental crisis, causing major damage to the ecosystem and potentially harmful effects to human health (Jambeck et al., 2015).

To address plastic pollution, there is a need to boost plastic recycling rates (PEW Charitable Trusts; & SYSTEMIQ, 2020). While plastic recycling rates have generally been trending upwards over the years, plastic recycling rates remain low globally at around 18% (OECD, 2018). A major challenge contributing to low recycling rates is the inability to properly sort recyclable plastics without contamination from other waste, which affects the quality and market value of recycled plastic products. Furthermore, plastic sorting has traditionally relied on a combination of manual labor and physical methods (Dodbiba & Fujita, 2004), which cannot be scaled up efficiently to reap the benefits of economies of scale due to high labor costs.

In recent years, the chemometric analysis of non-destructive spectroscopic data has been increasingly studied as an automated approach to improve plastic sorting systems (Araujo-Andrade et al., 2021). Widely used spectroscopic data includes infrared (IR), Raman and laser-induced breakdown spectroscopy (LIBS) (Neo et al., 2022). IR spectroscopy can be further broken down into near-infrared (NIR) and mid-infrared (MIR). IR spectroscopy measures the absorption/reflectance of IR radiation by chemical bonds within the plastic molecule. Raman spectroscopy measures the inelastic scattering of photons after excitation of plastic molecules by a laser. IR and Raman are often referred to as complimentary techniques, since Raman spectroscopy is active for chemical bonds with a change in polarizability, while IR spectroscopy is active for chemical bonds with a change in dipole moment. LIBS measure the elemental composition of plasma generated by laser pulses on the plastic. Each of these techniques produces a spectrum that serves as a molecular fingerprint to differentiate between plastic of different resin type.

Chemometric analysis can be realized with machine learning techniques. Traditional machine learning techniques like partial least square (PLS), k-nearest neighbor (kNN) and support vector machine (SVM) are popular options. Deep learning is a machine learning technique utilizing deep neural networks in an iterative learning process to determine the

* Corresponding author.
*E-mail address:* edward.neo@warwick.ac.uk (E.R.K. Neo).

https://doi.org/10.1016/j.resconrec.2022.106718
Received 27 May 2022; Received in revised form 28 September 2022; Accepted 12 October 2022
Available online 21 October 2022

neuron weights that can best map data in the input layer to the output layer. This is achieved through neurons in the hidden layer that consist of mathematical functions that apply different weightage to different parts of the data in the input layer. Deep learning techniques are considered state-of-the-art in many fields but have not seen the same level of uptake in chemometrics (Neo et al., 2022).

### 1.1. Literature review

The use of chemometrics for classification of plastic using non-destructive spectroscopic data is well established. One of the most popular technique is principal component analysis (PCA). In PCA, the data undergoes dimensionality reduction to principal components that explain the variance within the data. Hence, similar data points would be clustered together on a PCA plot. PCA was used in earlier chemometrics work to identify the potential on distinguishing plastics by IR spectra (De Biasio et al., 2010) and LIBS spectra (Grégoire et al., 2011). It also continues to be used as a pre-processing technique prior to machine learning model training (Musu et al., 2019; Yan et al., 2021; Yang et al., 2020; Zhu et al., 2019)

Supervised machine learning techniques include PLS, kNN and SVM are also popular chemometric techniques. For PLS, latent variables are constructed that best explain the relationship between the spectral data and the output label. This technique has traditionally been popular as a chemometric tool, and can be used for both classification and regression tasks (Calvini et al., 2018; da Silva & Wiebeck, 2020; K. Liu et al., 2019; Pieszczek & Daszykowski, 2019; Saeki et al., 2003; Sato et al., 2002). The kNN algorithm classifies data based on the majority class of its surrounding neighbors (Costa et al., 2017; Yang et al., 2020). SVM algorithm works based on the construction of a hyperplane that serves as a decision boundary between different classes (Musu et al., 2019; Yang et al., 2020; Yu et al., 2014; Zhu et al., 2019). These machine learning techniques have been found to give good results with IR spectra (Bonifazi et al., 2014; Calvini et al., 2018; Karaca et al., 2013; Rani et al., 2019; Said et al., 2020; S Serranti et al., 2020; Silvia Serranti et al., 2012, 2015; Ulrici et al., 2013; Wu et al., 2020; Yang et al., 2020; Zhu et al., 2019), Raman spectra (Allen et al., 1999; L. Chen et al., 2017; Musu et al., 2019; Silva & Wiebeck, 2019) and LIBS spectra (Costa et al., 2017; Junjuri et al., 2019; Vahid Dastjerdi et al., 2018; Yan et al., 2021; Yu et al., 2014).

The use of artificial neural networks for chemometric analysis of plastic has also been studied with IR spectra (Feldhoff et al., 1997; Wienke et al., 1995; Yang et al., 2020), Raman spectra (Musu et al., 2019; Roh et al., 2017) and LIBS spectra (Boueri et al., 2011; Junjuri & Gundawar, 2019, 2020; Roh et al., 2018). These works generally used basic three-layered neural network architecture, containing only one hidden layer. With the advances in deep learning in recent years, some recent works have applied deep learning to more challenging tasks, such as mixed polymers classification (Stiebel et al., 2018) and classification of plastic from different manufacturers (Peng et al., 2021).

Despite well-established methodologies for chemometric-based classification of plastic, the datasets used in the above studies are limited as there is insufficient representation of plastic types in the dataset used for training the models and lack diversity of samples within each class. These datasets may not sufficiently represent the heterogeneity of samples received at waste sorting facilities. Hence, the high accuracies reported in the literature may not translate well into an industrial setting.

Environmental weathering of plastics due to conditions like sunlight and moisture results in degradation which decreases the plastic quality. While it has been shown that weathered plastic samples can be distinguished from near infrared spectra (Chen et al., 2021), the use of chemometrics to automatically classify weathered samples have not been well studied. As there are more subtle differences in spectral features, deep learning could be a solution to this classification task, since it is able to learn more intricate features as compared to traditional machine learning methods (LeCun et al., 2015).

In an industrial setting, NIR spectroscopy has traditionally been the spectrum of choice for application in plastic sorting lines due to the use of indium gallium arsenide (InGaAs) based detectors which are fast and sensitive for in-line systems (Neo et al., 2022). However, recent advances have seen the development of high-speed MIR, Raman and LIBS spectrometers that can be applied in industrial sorting lines as well. For instance, an array of specialized Raman spectrometers was used to identify plastic on a conveyor belt moving at 100 m/s (Musu et al., 2019). Commercial MIR hyperspectral cameras and LIBS sorting sensor have also recently entered the market (Ocean Insight, n.d.; Specim, 2020). Hence, this presents an opportune time to develop the chemometric techniques for sorting plastic based on other types of spectral data.

### 1.2. Aim and scope

In this study, deep learning was used for chemometric analysis of open-sourced FTIR and Raman polymer databases from multiple sources (Baskaran & Sathiavelu, 2020; Cowger et al., 2021; Dong et al., 2020; Munno et al., 2020). Due to a lack of open-sourced LIBS database, LIBS was excluded from this study. Through this study, the suitability of different neural network architectures as chemometric analysis techniques in identifying recyclable plastics was determined, taking into account various complicating factors that will be present in a real-world scenario. The recyclable polymers in this paper were identified as polyethylene (PE), polyethylene terephthalate (PET) and polypropylene (PP). The three recyclable polymers represent the bulk proportion of plastic waste from postconsumer sources (Schyns & Shaver, 2020) which are commonly accepted at plastic recycling programs and typically require further sorting at material recovery facilities. Other polymers like polystyrene (PS) and polyvinylchloride (PVC) were excluded from the recyclable polymers list due to the low densities of expanded polystyrene foams and release of toxic chlorinated products respectively. Other types of plastics commonly used in Waste Electrical and Electronic Equipment (WEEE) were also excluded as there are typically more specialized collection systems in place for WEEEs. The higher data availability with PE, PET and PP for both weathered and unaged polymers also allow for derivation of deeper insights. The study contributes to the literature through 1) development of deep learning techniques to improve differentiation of polymer sorting and 2) exploration of deep learning techniques in identifying weathered polymer samples.

## 2. Methods and materials

This section describes the workflow for this paper, which includes different model architectures and the experimental approach, dataset acquisition and pre-processing methods,

### 2.1. Model architecture

The classification task at hand involves separating recyclable polymers (PE, PET and PP) from a list of over 20 other polymers (Table S1) using spectral data. This presents a certain degree of difficulty, as there could be contamination from polymers with spectral data that are harder to distinguish from recyclable polymers. Drawing inspiration from the deep decision network developed by Murthy et al. (2016) for image classification task, which involves an algorithm to successively group training data automatically into clusters at various stages for an expert network to handle, we developed a novel architecture known as the PolymerSpectraDecisionNet (PSDN) for this classification task, comprising two neural network modules arranged in a tree like structure (Fig. 1). The first module is a neural network trained to classify spectral data into two classes – recyclable and non-recyclable, which helps to filter the dataset into a smaller subset with less non-recyclable polymers. The spectra predicted as recyclable from the first module were then

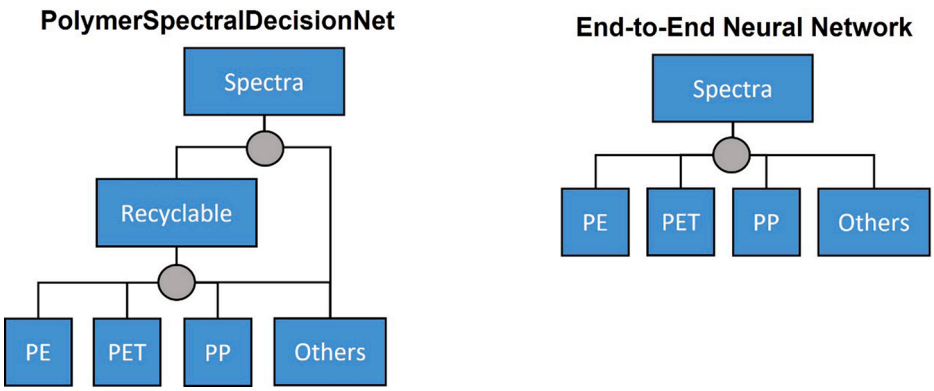


**Fig. 1.** PSDN and E2E network approach. Grey circle represents a neural network. To account for non-recyclable polymers that were wrongly classified as recyclable in the first neural network, the second neural network also features a non-recyclable class.

passed through a second neural network, which can then serve as an expert network to classify the polymers into their individual classes. To account for non-recyclable polymers that were wrongly classified as recyclable in the first neural network, the second neural network also features a non-recyclable class, allowing for two points of rejection of non-recyclable polymers, which could help to improve the purity of the sorted plastic stream. The approach was compared to a more traditional end-to-end neural (E2E) network.

Several neural network architectures were studied for both the PSDN and E2E approach. Convolutional neural networks (CNN) are effective for analysis of 1D data, achieving state-of-the-art performance at low computational cost (Kiranyaz et al., 2021). In this study, four different CNN architectures that have shown good results with spectral data were used (Ng et al., 2019, 2020; Riese & Keller, 2019; Wang et al., 2020; Zhang et al., 2019). Artificial neural network (ANN) was also included to serve as a benchmark architecture.

### 2.1.1. *Artificial neural networks*

ANNs utilize fully connected neurons in hidden layers to map an input vector representing the data to the output class. Each of the neurons contains a function that applies a weight to different parts of the input, and together all the neurons help to learn a complex function. ANNs have been widely used for plastic classification from Raman spectrum (Musu et al., 2019) and other spectroscopic methods (Boueri et al., 2011; Junjuri & Gundawar, 2019, 2020; Yang et al., 2020). Hence, it serves as a useful benchmark to evaluate the effectiveness of CNN for this classification task. In this work, an ANN with 3 hidden layers with 4096 neurons in each hidden layer was used.

### 2.1.2. *Convolutional neural networks*

CNN architectures are built with at least two types of layers – convolutional layers that extracts features from the input data and fully connected layers that are essentially ANNs. Some CNNs also contain pooling layers that helps in dimension reduction to reduce computational demands. CNNs have not been thoroughly explored for plastic classification tasks from spectrum data (Stiebel et al., 2018), but have been applied for other tasks, such as soil and food quality prediction (Y.-Y. Chen & Wang, 2019; Ng et al., 2019, 2020; Riese & Keller, 2019; Wang et al., 2020; Zhang et al., 2019). The basic CNN architecture, adapted from Ng et al. (2020) is illustrated in Fig. 2, while the

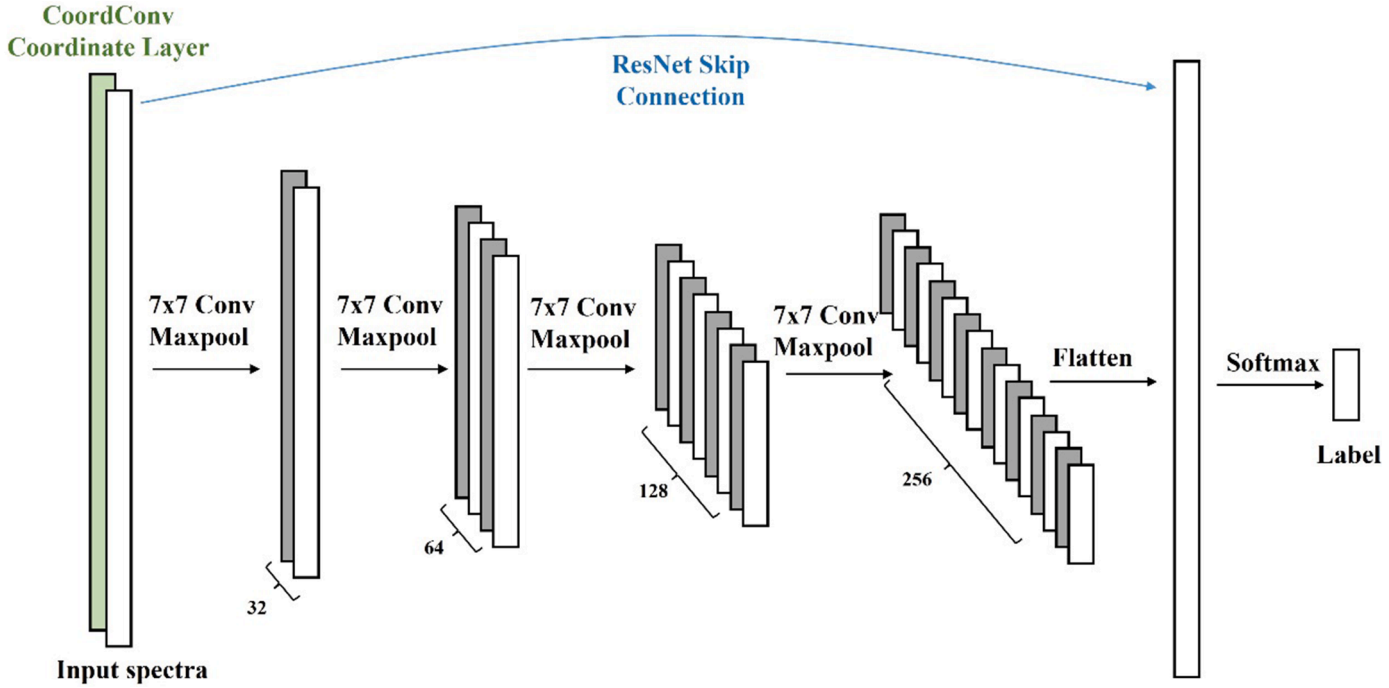


**Fig. 2.** Architecture for CNN, CoordConv and ResNet.

hyperparameters are shown in Table S2. It is composed of four convolution layers, four pooling layers and three fully connected layers. Variations of the basic CNN architecture includes the CoordConv and residual network (ResNet) which is adapted from Riese & Keller (2019) and inception Net adapted from Wang et al. (2020) and Zhang et al. (2019).

In CoordConv, the input data is extended by concatenating a hard-coded coordinate channel with a range of [−1, 1] (R. Liu et al., 2018). This removes elements of translational invariance during the learning process, which is suitable for this task since each Raman shift is fixed to an index in the input data. The transformed data is then passed through the same basic CNN architecture.

In ResNet, a skip connection is formed between an input of an earlier previous layer and the output of deeper layers which can help in learning identity mapping (He et al., 2016). In this work, the residual connection is formed between the input layer and the output of the fourth pooling layer before flattening into the first fully connected layer.

In Inception Net, an inception block is utilized which concatenates the output of four parallel branches –1 × 1 convolution, 3 × 1 convolution, 5 × 1 convolution and max-pooling. The original Inception Net created by Szegedy et al. (2015) for image recognition coupled 1 × 1 convolutions in the branches for dimension reduction to reduce the computational demands. However, since the data used in this work is just one dimensional, the strain on computational resources is much reduced. Therefore, a naïve inception block was used instead without the 1 × 1 convolutions for dimension reduction. The architecture for the Inception Net used in this work is shown in Fig. 3 and the hyperparameters are shown in Table S3.

### 2.2. Dataset description

There are two separate datasets built for the purpose of experimentation, namely the Raman dataset and FTIR dataset.

#### 2.2.1. Raman dataset

Three different open access Raman polymer spectral databases were used to generate the Raman dataset for this work. The first database is the Open Specy Raman reference library (Cowger et al., 2021), from which the Raman spectra of 266 polymer samples were obtained. The second database is the Raman database of standard and weathered microplastics (RDSP & RDWP) created by Dong et al. (2020), from which 173 polymer samples were obtained. The final database is the spectral libraries of plastic particles (SLoPP & SLoPP-E) created by Munno et al. (2020), from which 261 polymer samples were obtained. The three combined databases gave a total of 700 polymer samples.

Each polymer sample was labelled according to the 'type' and 'weathering'. The 'type' label consisted of one of 4 classes – *PE, PET, PP* and *others*. These three polymers (PE. PET and PP) were specifically labelled as they are the most widely recycled plastics (Locock et al., 2017). There are over 20 different polymers grouped under the 'others' label; these are summarized in Table S3. The 'weathering' label consists of 2 classes, weathered and unaged. The unaged samples may refer to either virgin plastics or postconsumer plastic waste that would be thrown into general or recycling bins. The weathered samples have gone through controlled weathering experiments (Chabuka & Kalivas, 2020) or have been naturally weathered in the environment over prolonged periods of time (Baskaran & Sathiavelu, 2020; Dong et al., 2020; Munno et al., 2020) The dataset characteristics are summarized in Table 1, while information related to sample and equipment is furnished in Table S4.

#### 2.2.2. FTIR dataset

Two different open access FTIR polymer spectral databases were used to generate the Raman dataset for this work. The first database is the Open Specy FTIR reference library (Cowger et al., 2021), from which

**Table 1**
Raman dataset characteristics. The number of weathered samples in each database is indicated in parentheses.

| | Raman shift ($cm^{-1}$) | Labels PE | PET | PP | Others | Total |
|---|---|---|---|---|---|---|
| Open Specy | 150 – 3000<br>300 – 2000<br>300 – 3200 | 42 | 12 | 16 | 196 | 266 |
| RDSP & RDWP | 200 – 3500 | 74 (72) | 16 (10) | 54 (51) | 29 (22) | 173 (155) |
| SLoPP & SLoPP-E | 100 – 3500<br>100 – 2000 | 50 (26) | 32 (13) | 38 (21) | 141 (53) | 261 (113) |
| **Total** | | **166 (98)** | **60 (23)** | **108 (72)** | **366 (75)** | **700 (268)** |

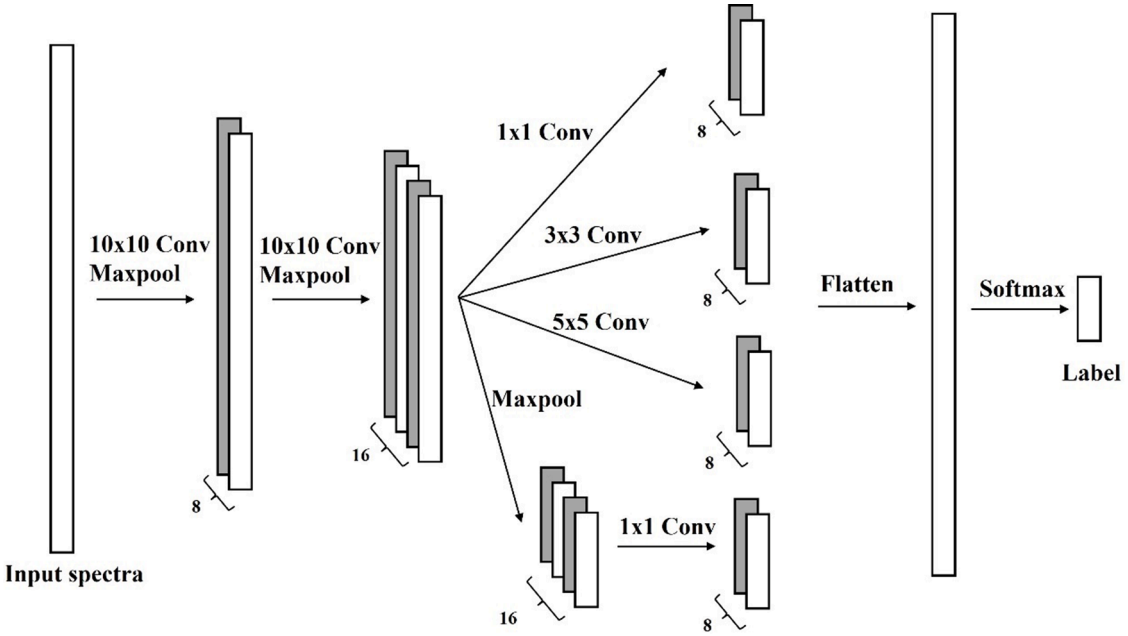


**Fig. 3.** Inception net architecture.

the ATR-FTIR spectra of 626 polymer samples were obtained. The second database is an ATR-FTIR database of food packaging plastics created by Baskaran & Sathiavelu (2020), from which 96 polymer samples were obtained. The two combined databases gave a total of 722 polymer samples.

Similar to the Raman dataset, each polymer sample was labelled according to the 'type' and 'weathering'. However, the 'type' label consists of 5 classes this time, where the *PE* class is further split into *HDPE* and *LDPE* because the distinction between both types of *PE* were identified in the FTIR databases. The dataset characteristics are summarized in Table 2, while information related to sample and equipment is furnished in Table S5.

### 2.3. Pre-processing

As the dataset is built from separate databases, it contains a variety of spectral range, each with different spectral resolutions. In order to use all the spectra in the database for the same deep learning model and minimize the impact of variation in spectral data, a variable-length spectral mapping (VLSM) algorithm is proposed. The algorithm maps each spectral data into a 1D array of 4000 numbers, representing a unit of Raman shift or wavenumber in $cm^{-1}$. Missing spectral information is replaced with a zero. This ensures that each spectral peak corresponding to specific chemical bond vibrational frequency will be at the same index in the input data, regardless of the raw spectral range.

The VLSM algorithm consists of three main steps. Firstly, interpolation is applied to resize the data. Secondly, the data is pre-processed with standard normal variate, asymmetric square baseline correction and Savitzky-Golay smoothing (window size 9 and third order polynomial), to remove noise from the spectral data (Wang et al., 2020) and background fluorescence in the Raman spectrum (Dong et al., 2020). Lastly, the data is mapped into an empty 1D array of size 4000. The dataset was then randomly split into a ratio of 75: 15: 10 (training, evaluation, testing). Since the test set is 10% of the total dataset, a 10-fold cross validation was performed. Furthermore, for each fold, each neural network was trained for a total of 10 runs to ensure reliability of the results. Out of the 10 runs in each fold, the model that performed the best on the validation set was chosen for evaluating the test set.

### 2.4. Evaluation

A confusion matrix for the test dataset was used to evaluate the model performances, normalized with respect to the total number of samples in each class. From the confusion matrix, the overall accuracy, and precision and recall (Eq. 1) for each plastic type could be determined. Precision is the proportion of all positive predictions that are correct, which gives an indication of the potential contamination level for the recyclable plastics after classification. Recall is the proportion of all actual positive that are correctly identified, which gives an indication of how much of each of the recyclable plastics can be recovered.

$$Accuracy = \frac{TP + TN}{TP + TN + FP + FN}$$

**Table 2**
FTIR dataset characteristics. The number of weathered samples in each database is indicated in parentheses.

| Database | Wavenumber ($cm^{-1}$) | Labels HDPE | LDPE | PET | PP | Others | Total |
|---|---|---|---|---|---|---|---|
| Open Specy | 400/675 – 4000 $cm^{-1}$ | 147 (68) | 12 | 146 (73) | 10 | 311 | 626 |
| Baskaran | 650 – 4000 $cm^{-1}$ | 0 | 29 (10) | 21 (5) | 37 (5) | 9 | 96 |
| **Total** | | **147 (68)** | **41 (10)** | **167 (78)** | **47 (5)** | **320** | **722** |

$$Precision = \frac{TP}{TP + FP}$$

$$Recall = \frac{TP}{TP + FN} \quad (1)$$

where TP = True Positive, TN = True Negative, FP = False Positive, FN = False Negative.

The evaluation metrics of accuracy, precision and recall are then averaged over the 10 folds to give a more generalizable result.

## 3. Results and discussion

This section will discuss the results from the use of various neural network architecture for chemometric analysis of the Raman and FTIR datasets. For all neural network architectures, a rectified linear (ReLu) activation function was used, while the output layer contains a softmax classifier. The weight of the neurons in the network was initialized with the Xavier initialization. The loss function used was the mean squared error. The models were trained with an Adam optimizer with a learning rate of 0.001 for 50 epochs. The workflow is implemented using the Python PyTorch library on an Intel(R) Xeon(R) CPU E5-2690 (8 Cores, 32GB RAM) with a Nvidia Titan Xp graphics card (1GB RAM), which took between 15 and 30 s for training of a model and 1–2.5 ms for inference of one set of data.

### 3.1. Effects of preprocessing

Preliminary experiments were conducted to investigate the effect of preprocessing on model performance, summarized in Table 3. To evaluate the effectiveness of the mapping step, a control experiment was also performed to exclude the mapping step during preprocessing. The control experiment performed significantly worse than all other methods of preprocessing, which points to the importance of the mapping step to handle spectral data of different spectral ranges. Without the mapping step, the dataset requires translational invariance. This explains the poor accuracy of ~0.4 for the CoordConv models since elements of translational invariance are removed during the learning process.

Applying interpolation followed by noise removal gave the better accuracy than the converse in all cases. This process flow helps to smoothen out any noise that may have been generated during the interpolation step. In the case of Raman spectra, bicubic interpolation gave better results, while bilinear interpolation gave better results for FTIR. However, the accuracies across both cases were largely comparable, which suggests that the type of interpolation applied in the VLSM algorithm did not affect the result significantly. For standardization purpose, bilinear interpolation algorithm was chosen for all spectral data.

### 3.2. Quantitative analysis

The results of the selected experimental runs of PSDN with Raman and FTIR spectra are summarized in Table 4. Since the focus of the classification task is sorting out the recyclables that are most commonly found at material recovery facilities from waste at general recycling collection points, the precision and recall metrics are presented as weighted average of the recyclable classes (PE, PET and PP), rather than the entire dataset. The full results are presented in Table S6.

Overall, the PSDN model performed better than the E2E models, with the best performing models being the ResNet-Inception Net model for Raman with an accuracy of 0.949, and CoordConv-Inception Net model for FTIR with an accuracy of 0.967. The relative performance of the PSDN models to the E2E models is evaluated by taking the average of the difference between each of the five model in the second node with and without the first node. Utilizing the PSDN models gave a pronounced effect in terms of precision and recall. The precision in the PSDN models

**Table 3**
Effects of preprocessing on accuracy of E2E models built with Raman and FTIR spectra. Reported results represent the mean and standard variation across 10-folds.

| Spectra | Preprocessing | E2E model accuracy | | | | |
|---|---|---|---|---|---|---|
| | | ANN | CNN | CoordConv | ResNet | Inception Net |
| Raman | Bilinear Interpolation – Noise Removal - Mapping | 0.901 ± 0.033 | **0.936 ± 0.026** | 0.923 ± 0.021 | 0.930 ± 0.030 | 0.941 ± 0.028 |
| | Bicubic Interpolation – Noise Removal - Mapping | **0.907 ± 0.050** | 0.936 ± 0.036 | **0.924 ± 0.032** | **0.936 ± 0.035** | **0.943 ± 0.019** |
| | Noise Removal – Bilinear Interpolation – Mapping | 0.896 ± 0.037 | 0.911 ± 0.030 | 0.919 ± 0.031 | 0.924 ± 0.028 | 0.934 ± 0.028 |
| | (Control) Bilinear Interpolation – Noise Removal | 0.589 ± 0.051 | 0.509 ± 0.094 | 0.410 ± 0.108 | 0.514 ± 0.117 | 0.513 ± 0.081 |
| FTIR | Bilinear Interpolation – Noise Removal - Mapping | 0.947 ± 0.031 | **0.954 ± 0.015** | **0.961 ± 0.017** | **0.956 ± 0.026** | **0.964 ± 0.021** |
| | Bicubic Interpolation – Noise Removal - Mapping | **0.951 ± 0.016** | 0.947 ± 0.016 | 0.956 ± 0.02 | 0.956 ± 0.034 | 0.958 ± 0.021 |
| | Noise Removal – Bilinear Interpolation – Mapping | 0.932 ± 0.029 | 0.929 ± 0.051 | 0.935 ± 0.06 | 0.951 ± 0.034 | 0.958 ± 0.014 |
| | (Control) Bilinear Interpolation – Noise Removal | 0.663 ± 0.071 | 0.642 ± 0.179 | 0.412 ± 0.209 | 0.649 ± 0.167 | 0.64 ± 0.189 |

**Table 4**
Average accuracy, precision and recall from 10-fold cross validation with Raman and FTIR spectra. Reported results represent the mean and standard variation across 10-folds.

| Node 1 | Node 2 | Raman | | | FTIR | | |
|---|---|---|---|---|---|---|---|
| | | Accuracy | Precision | Recall | Accuracy | Precision | Recall |
| CoordConv | ANN | 0.920 ± 0.024 | 0.921 ± 0.057 | 0.882 ± 0.075 | 0.951 ± 0.023 | 0.941 ± 0.123 | 0.953 ± 0.115 |
| | CNN | 0.939 ± 0.026 | 0.939 ± 0.009 | 0.918 ± 0.059 | 0.960 ± 0.018 | 0.950 ± 0.074 | 0.956 ± 0.053 |
| | CoordConv | 0.934 ± 0.023 | 0.933 ± 0.069 | 0.922 ± 0.086 | 0.964 ± 0.015 | 0.957 ± 0.065 | 0.956 ± 0.085 |
| | ResNet | 0.929 ± 0.026 | 0.947 ± 0.022 | 0.897 ± 0.049 | 0.961 ± 0.025 | 0.958 ± 0.067 | 0.952 ± 0.157 |
| | Inception Net | 0.941 ± 0.028 | 0.950 ± 0.010 | 0.920 ± 0.041 | **0.967 ± 0.019** | 0.956 ± 0.065 | 0.970 ± 0.081 |
| ResNet | ANN | 0.929 ± 0.029 | 0.934 ± 0.070 | 0.893 ± 0.054 | 0.956 ± 0.016 | 0.955 ± 0.103 | 0.948 ± 0.114 |
| | CNN | 0.947 ± 0.023 | 0.949 ± 0.015 | 0.930 ± 0.009 | 0.960 ± 0.010 | 0.949 ± 0.106 | 0.957 ± 0.046 |
| | CoordConv | 0.943 ± 0.023 | 0.936 ± 0.052 | 0.935 ± 0.032 | 0.963 ± 0.013 | 0.959 ± 0.052 | 0.953 ± 0.084 |
| | ResNet | 0.937 ± 0.026 | 0.947 ± 0.068 | 0.913 ± 0.047 | 0.960 ± 0.024 | **0.961 ± 0.070** | 0.947 ± 0.150 |
| | Inception Net | **0.949 ± 0.026** | **0.955 ± 0.029** | 0.935 ± 0.052 | 0.964 ± 0.015 | 0.954 ± 0.095 | 0.971 ± 0.047 |
| NA (E2E) | ANN | 0.901 ± 0.033 | 0.872 ± 0.041 | 0.905 ± 0.057 | 0.947 ± 0.031 | 0.930 ± 0.180 | 0.958 ± 0.122 |
| | CNN | 0.936 ± 0.026 | 0.922 ± 0.010 | 0.935 ± 0.026 | 0.954 ± 0.015 | 0.938 ± 0.131 | 0.961 ± 0.051 |
| | CoordConv | 0.923 ± 0.021 | 0.898 ± 0.039 | 0.940 ± 0.051 | 0.961 ± 0.017 | 0.951 ± 0.076 | 0.959 ± 0.086 |
| | ResNet | 0.930 ± 0.030 | 0.934 ± 0.052 | 0.917 ± 0.071 | 0.956 ± 0.026 | 0.950 ± 0.073 | 0.952 ± 0.157 |
| | Inception Net | 0.941 ± 0.028 | 0.934 ± 0.052 | **0.942 ± 0.076** | 0.964 ± 0.021 | 0.947 ± 0.094 | **0.979 ± 0.058** |
| Voting Ensemble | | 0.940 ± 0.025 | 0.936 ± 0.028 | 0.941 ± 0.054 | 0.965 ± 0.020 | 0.952 ± 0.083 | 0.973 ± 0.071 |

improved by 0.017 – 0.032 for Raman and 0.004 – 0.012 for FTIR, while the recall dropped by −0.007 – −0.025 for Raman and −0.003 – −0.021 for FTIR. The tree like structure in the PSDN offers two points for rejection of non-recyclable plastic. This could result in lower contamination of recyclable plastic, but also increasing the likelihood of a recyclable plastic being classified as 'others', hence reducing the recovery of recyclable plastic. In the context of the plastic recycling industry, blending of different polymers could adversely affect the quality of recycled plastic (La Mantia et al., 2017), which points towards PSDN as the better approach due to the improved precision.

For the end-to-end (E2E) approach, the CNN-based models performed better than ANN across all three metrics of accuracy, precision and recall. Since CNNs are composed of both convolutional and fully-connected layers, there is a fusing of classification and feature extraction operations, hence improving the model performance (Kiranyaz et al., 2021). Comparing the four different CNN architectures, Inception Net consistently performs the best, with an average overall accuracy of 0.941 for Raman spectra and 0.964 for FTIR spectra. This is consistent with a previous study which found that Inception Net model performs better than other CNN models on four different near-infrared spectroscopic datasets (Zhang et al., 2019).

It is of interest to examine if the better performance of PSDN over E2E networks could be due to different model architectures picking up slightly different features in the dataset. To test this theory, an ensemble network was built using the five E2E models. The output of the ensemble network was determined either through voting, or by taking the majority output from the individual models.

The last row of Table 4 summarizes the results of the ensemble network. Comparing the voting ensemble to the best performing E2E model of inception net, the overall model performance is similar, but there is a slightly higher precision and slightly lower recall. This supports the earlier theory that each of the networks is able to learn different features from the dataset.

Across the board, models built using FTIR spectra performed better than models built using Raman spectra. Furthermore, despite the 'PE' class being split into 'HDPE' and 'LDPE' for the FTIR dataset, there was no misclassification between HDPE and LDPE samples (Figure S1). This shows that the side chains $CH_3$ symmetric bend at ~1375 $cm^{-1}$ that is present at higher intensity in the FTIR spectra of LDPE as compared to HDPE due to higher side chain branching (Jung et al., 2018) (highlighted in a red box in Fig. 4) could be detected using chemometric techniques, allowing for differentiation between HDPE and LDPE. The relatively poorer performance of the model built with Raman spectra could be due to the presence of weathered microplastics in the Raman dataset (Table S4), which tends to be characterized by strong background fluorescence in the spectrum caused by surface contamination (Dong et al., 2020). Even after baseline correction during the preprocessing stage, there could be some unintentional features that do not represent the polymer. This will be further discussed in the subsequent qualitative analysis section.

### 3.3. Qualitative analysis

The average spectra from the FTIR and Raman dataset used in this paper is displayed in Fig. 4 as the orange dotted line, with a reference virgin sample from the NIST spectral database as a solid blue line. All the spectra were passed through the variable length spectral mapping algorithm. The indicative main peaks for each polymer and their corresponding functional groups are presented in Table S7.

The average FTIR spectra largely resembles the virgin sample for the PET samples, with the exception of peaks below 500 $cm^{-1}$ which were out of range in the FTIR dataset. For the polyolefins, some differences were observed, namely the presence of regions of overlapping peaks from 1000 to 1250 $cm^{-1}$ and in the carbonyl region (1600–1800 $cm^{-1}$).

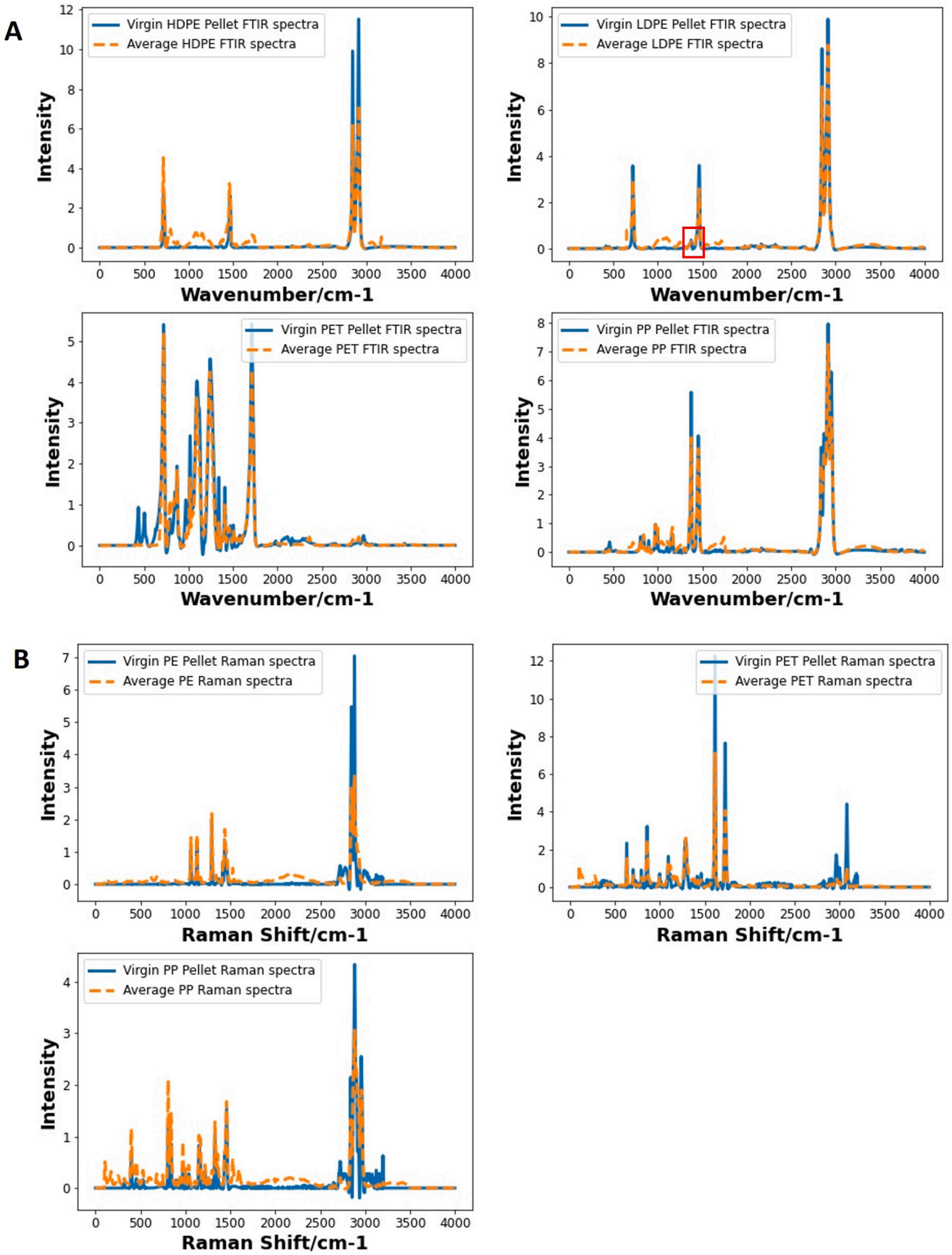


**Fig. 4.** Comparison of average A) FTIR and B) Raman spectra of polymers in the dataset to virgin polymer. Red box highlights $CH_3$ symmetric bend at ~1375 $cm^{-1}$ that is present in higher intensity in the FTIR spectra of LDPE compared to HDPE.

A zoomed in portion of the FTIR spectrum is presented in Figure S2. These differences could be indicative of the presence of weathered polymers within the dataset and are consistent with previous spectroscopic investigation studies (Hamzah et al., 2018; Zvekic et al., 2022). The region from 1000 to 1250 $cm^{-1}$ are formed from overlapping bands of C-O bonds in ether and ester groups. The region in the range of 1600 cm–1800 $cm^{-1}$ are composed of overlapping carbonyl peaks (1700–1800 $cm^{-1}$) and vinyl C=C stretch (1600–1670 $cm^{-1}$), both which are known to form during weathering. Ketone and aliphatic esters are formed during photo-oxidation, while further photolysis of the ketone group via a free radical process results in the formation of vinyl group. This is further supported by the peak in the range of 800–900 $cm^{-1}$, which corresponds to the C-H bend of the vinylidene H (Hamzah et al., 2018). Another possible contributing factor to the differences in virgin spectra and our spectra is the presence of additives, such as antioxidants which are known to show a peak at 1744 $cm^{-1}$ (Zheng et al., 2020).

On the other hand, the average Raman spectra differ significantly from the virgin sample. This is largely due to background fluorescence, which could completely obscure the characteristic peaks in some instances. Colored additives, weathering or contaminants can all contribute to the fluorescence phenomenon (Dong et al., 2020), which would not be present in colorless virgin polymer pellets. Hence, there are greater variations within the polymer Raman spectral dataset, which likely contributed towards the poorer performance relative to FTIR spectral dataset.

It is of interest to qualitatively examine the spectra of polymers that were misclassified to determine possible explanation for the misclassifications. This could serve to inform the construction of dataset used for training of future deep learning models. In this case, only false positive misclassifications are flagged, since they are more of a concern in terms of contamination of recyclable plastic. Table 5 summarizes the main misclassifications that were observed for the best performing model with both Raman and FTIR dataset, namely the ResNet-Inception Net PSDN and CoordConv-Inception Net PSDN respectively.

A large majority of the false positive errors are misclassifications as polyolefins (PE and PP), likely due to similar spectral peaks relating to the $CH_2$ present in the carbon backbones of the polymers. This occurs despite the presence of many other spectral peaks in the misclassified polymers that would not be typically present in polyolefins sample. This suggests a very high weightage being assigned to the region of IR and Raman spectra associated with $CH_2$ symmetric stretch (2920 – 2935 $cm^{-1}$) and $CH_2$ asymmetric stretch (2840 – 2860 $cm^{-1}$) towards positive prediction of polyolefins. One possible method to reduce such false positive error is the use of attention mechanism within the deep learning architecture, allowing the model to selectively focus on important parts of the spectral data.

**Table 5**
Main misclassified polymers from the IR and Raman polymer dataset.

| Polymer | Misclassification | Spectra | Possible explanation |
|---|---|---|---|
| PE | PP | Raman | $CH_2$ asymmetric and symmetric stretch of PE and PP lies in similar region |
| PP | PE | Raman | |
| Polystyrene | PE | IR, Raman | $CH_2$ asymmetric and symmetric stretch of polystyrene lies in similar region as that of PE and PP |
| | PP | IR | |
| Methacrylate | PE | IR | C=O stretch in ester bond of methacrylate lies in similar region to that of PET. $CH_2$ asymmetric and symmetric stretch of methacrylate lies in similar region as that of PE |
| | PET | Raman | |
| Ethylene vinyl acetate | PE | IR, Raman | $CH_2$ asymmetric and symmetric stretch of ethylene part of polymer lies in similar region as that of PE |
| Phenoxy resin | PET | IR | C-O stretch of phenoxy lies in similar region as that of PET |
| Cotton/ Cellulose | PE, PP | Raman | $CH_2$ asymmetric and symmetric stretch of in carbon backbone lies in similar region as that of PE |

### 3.4. Differentiating weathering and unaged

After sorting of polymers into their respective classes, it is important to differentiate between weathered and unaged polymer samples such that high quality polymers can be isolated for recycling purposes, to maintain the quality of plastic recyclate. Deep learning was explored as a tool for further sorting of the polymers, using the five neural network architectures previously used to classify polymer by resin type. Each neural network was only trained on one type of polymer spectral data in a 90:10 ratio (training, testing) with 10-fold cross validation. Due to the small sample size of weathered LDPE and PP polymers (10 and 5 respectively) in the FTIR database, there will not be a good enough representation of weathered samples in the test sets for all 10-folds, hence they have been removed from this experiment. The results are summarized in Table 6.

On the whole, FTIR spectra appears to be more promising for separating weathered and unaged polymer samples. Interestingly, it can be observed that ANN generally outperforms the other CNN architecture for this classification task, which is the reverse of earlier experiments for classification by resin types.

In the Raman dataset, the best performing polymers are PE and PP with accuracies of 0.866 and 0.845 respectively. From the Raman spectra in Fig. 5, it can be observed that weathered polyolefins samples shown a broad peak at around 2200 $cm^{-1}$, while the peaks in the fingerprint region between 0 and 1500 $cm^{-1}$ are generally of a lower intensity than the weathered counterpart. However, both weathered and unaged PET Raman spectra are very similar, which explains the poor accuracy of 0.621.

For the FTIR dataset, LDPE and PP polymers were removed from the study. Due to the small sample size of weathered LDPE and PP polymers (10 and 5 respectively), there will not be a good enough representation of weathered samples in the test sets for all 10-folds. The two remaining polymers, HDPE and PET achieved food results with accuracies of 0.954 and 0.906 respectively. The FTIR spectra in Fig. 5 shows clear

**Table 6**
Average accuracy of classifying unaged and weathered polymer samples with Raman and FTIR spectra. Reported results represent the mean and standard variation across 10-folds. LDPE and PP were excluded from FTIR results due to insufficient weathered sample size.

| Spectra | Model | Polymer HDPE | LDPE | PP | PET |
|---|---|---|---|---|---|
| Raman | ANN | **0.866 ± 0.075** | | **0.845 ± 0.109** | **0.621 ± 0.185** |
| | CNN | 0.818 ± 0.084 | | 0.728 ± 0.117 | 0.597 ± 0.115 |
| | CoordConv | 0.744 ± 0.082 | | 0.606 ± 0.122 | 0.547 ± 0.064 |
| | ResNet | 0.776 ± 0.077 | | 0.719 ± 0.166 | 0.589 ± 0.140 |
| | Inception Net | 0.853 ± 0.087 | | 0.749 ± 0.109 | 0.565 ± 0.097 |
| FTIR | ANN | 0.919 ± 0.055 | - | - | **0.906 ± 0.049** |
| | CNN | 0.938 ± 0.041 | - | - | 0.861 ± 0.051 |
| | CoordConv | 0.921 ± 0.036 | - | - | 0.851 ± 0.069 |
| | ResNet | 0.946 ± 0.038 | - | - | 0.883 ± 0.064 |
| | Inception Net | **0.954 ± 0.034** | - | - | 0.898 ± 0.057 |

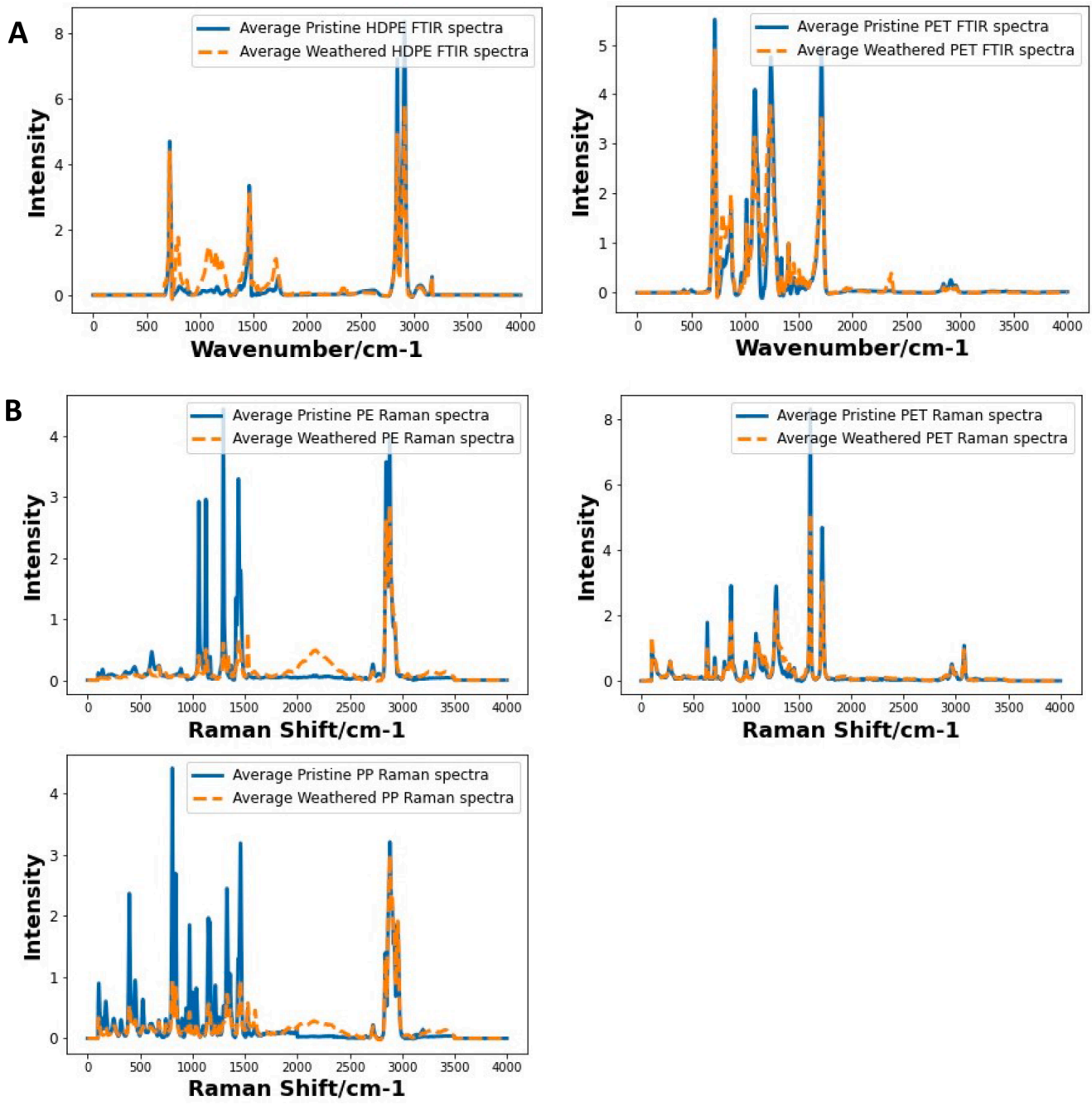


**Fig. 5.** Comparison of average unaged and weathered polymer samples for A) FTIR and B) Raman spectra.

differences in spectral features for the weathered HDPE and PET samples. A large majority of HDPE and PET data used in the FTIR dataset was from Chabuka & Kalivas (2020), which used lab-based techniques to simulate environmental weathering. The high accuracies also suggest that spectra from simulated weathered polymer samples may be a good representation of naturally weathered samples.

## 4. Conclusion

In conclusion, this work has demonstrated a deep learning methodology to effectively sort recyclable plastics from a wide range of over 20 different polymers based on FTIR and Raman spectral data obtained from various sources, achieving an accuracy of 0.967 for FTIR spectra and 0.949 for Raman spectra. Our PolymerSpectraDecisionNet gave higher precision than an end-to-end neural network architecture, potentially resulting in less contamination in the sorted plastic stream. Once the polymers have been sorted into their individual classes, a further neural network can be employed to identify weathered polymer samples that could compromise the quality of the plastic recyclate. Preliminary results were encouraging, as HDPE and PET weathered polymer samples could be differentiated from unaged samples based on the FTIR spectra with an accuracy of 0.954 and 0.906 respectively. This work represents a deeper exploration of using chemometrics for sorting of more diverse plastic samples as compared to the literature. Industrially, this can be applied at material recovery facilities for household wastes, to sort recyclable polymers into higher purity streams as compared to current physical, optical or even state-of-the-art NIR based sorting methods. Future work can be done to continue building on existing polymer spectral databases. This includes the building up Raman data for both HDPE and LDPE, having larger sample sizes of

other types of less common polymers, having a mix of unaged and weathered polymer samples and expanding the database with LIBS data as well. This would allow further exploration of deep learning techniques in sorting out weathered polymer samples from going into recycling, which would contribute towards circularity in the plastic industry.

## CRediT authorship contribution statement

**Edward Ren Kai Neo:** Writing – original draft, Data curation, Software, Methodology. **Jonathan Sze Choong Low:** Supervision, Writing – review & editing. **Vannessa Goodship:** Supervision, Writing – review & editing. **Kurt Debattista:** Resources, Supervision, Writing – review & editing.

## Declaration of Competing Interest

The authors declare that they have no known competing financial interests or personal relationships that could have appeared to influence the work reported in this paper.

## Supplementary materials

Supplementary material associated with this article can be found, in the online version, at doi:10.1016/j.resconrec.2022.106718.

## References


Allen, V., Kalivas, J.H., Rodriguez, R.G., 1999. Post-consumer plastic identification using Raman spectroscopy. Appl. Spectrosc. 53 (6), 672–681. http://as.osa.org/abstract.cfm?URI=as-53-6-672.

Araujo-Andrade, C., Bugnicourt, E., Philippet, L., Rodriguez-Turienzo, L., Nettleton, D., Hoffmann, L., Schlummer, M., 2021. Review on the photonic techniques suitable for automatic monitoring of the composition of multi-materials wastes in view of their posterior recycling. Waste Manag. Res. 39 (5), 631–651. https://doi.org/10.1177/0734242X21997908.

Baskaran, S., Sathiavelu, M., 2020. Application of attenuated total reflection - Fourier transform infrared spectroscopy to characterize the degradation of littered multilayer food packaging plastics. Vib. Spectrosc. 109, 103105 https://doi.org/10.1016/j.vibspec.2020.103105.

Bonifazi, G., Maio, F.Di, Potenza, F., Serranti, S, 2014. FT-IR spectroscopy and hyperspectral imaging applied to post-consumer plastic packaging characterization and sorting. Sensors 2014, 633–636. https://doi.org/10.1109/ICSENS.2014.6985078. IEEE.

Boueri, M., Motto-Ros, V., Lei, W.-Q., Ma, Qain-Li, Zheng, L.-J., Zeng, H.-P., Jin, Yu., 2011. Identification of polymer materials using laser-induced breakdown spectroscopy combined with artificial neural networks. Appl. Spectrosc. 65 (3), 307–314. http://as.osa.org/abstract.cfm?URI=as-65-3-307.

Calvini, R., Orlandi, G., Foca, G., Ulrici, A., 2018. Development of a classification algorithm for efficient handling of multiple classes in sorting systems based on hyperspectral imaging. J. Spectr. Imaging 7. https://doi.org/10.1255/jsi.2018.a13.

Chabuka, B.K., Kalivas, J.H., 2020. Application of a hybrid fusion classification process for identification of microplastics based on Fourier transform infrared spectroscopy. Appl. Spectrosc. 74 (9), 1167–1183. http://as.osa.org/abstract.cfm?URI=as-74-9-1167.

Chen, L., Jin, S., Li, W., 2017. Rapid identification of plastics based on Raman spectroscopy with the combination of support vector machine. In: 2017 16th International Conference on Optical Communications and Networks (ICOCN), pp. 1–3. https://doi.org/10.1109/ICOCN.2017.8121214.

Chen, X., Kroell, N., Dietl, T., Feil, A., Greiff, K., 2021. Influence of long-term natural degradation processes on near-infrared spectra and sorting of post-consumer plastics. Waste Manag. 136, 213–218. https://doi.org/10.1016/j.wasman.2021.10.006.

Chen, Y.-Y., Wang, Z.-B., 2019. End-to-end quantitative analysis modeling of near-infrared spectroscopy based on convolutional neural network. J. Chemom. 33 (5), e3122. https://doi.org/10.1002/cem.3122.

Costa, V.C., Aquino, F.W.B., Paranhos, C.M., Pereira-Filho, E.R., 2017. Identification and classification of polymer e-waste using laser-induced breakdown spectroscopy (LIBS) and chemometric tools. Polym. Test. 59, 390–395. https://doi.org/10.1016/j.polymertesting.2017.02.017.

Cowger, W., Steinmetz, Z., Gray, A., Munno, K., Lynch, J., Hapich, H., Primpke, S., De Frond, H., Rochman, C., Herodotou, O., 2021. Microplastic spectral classification needs an open source community: open specy to the rescue! Anal. Chem. 93 (21), 7543–7548. https://doi.org/10.1021/acs.analchem.1c00123.

da Silva, D.J., Wiebeck, H., 2019. Predicting LDPE/HDPE blend composition by CARS-PLS regression and confocal Raman spectroscopy. Polímeros 29 scielo.

da Silva, D.J., Wiebeck, H., 2020. Current options for characterizing, sorting, and recycling polymeric waste. Prog. Rubber Plast. Recycl. Technol. 36 (4), 284–303. https://doi.org/10.1177/1477760620918603.

De Biasio, M., Arnold, T., Mcgunnigle, G., Leitner, R., Balthasar, D., & Rehrmann, V. (2010). Detecting and discriminating PE and PP polymers for plastics recycling using NIR imaging spectroscopy. 7661. https://doi.org/10.1117/12.850065.

Dodbiba, G., Fujita, T., 2004. Progress in separating plastic materials for recycling. Phys. Sep. Sci. Eng. 13, 594923 https://doi.org/10.1080/14786470412331326350.

Dong, M., Zhang, Q., Xing, X., Chen, W., She, Z., Luo, Z., 2020. Raman spectra and surface changes of microplastics weathered under natural environments. Sci. Total Environ. 739, 139990 https://doi.org/10.1016/j.scitotenv.2020.139990.

Feldhoff, R., Wienke, D., Cammann, K., Fuchs, H., 1997. On-line post consumer package identification by NIR spectroscopy combined with a FuzzyARTMAP classifier in an industrial environment. Appl. Spectrosc. 51 (3), 362–368. https://doi.org/10.1366/0003702971940215.

Geyer, R., Jambeck, J.R., Law, K.L., 2017. Production, use, and fate of all plastics ever made. Sci. Adv. 3 (7), e1700782 https://doi.org/10.1126/sciadv.1700782.

Grégoire, S., Boudinet, M., Pelascini, F., Surma, F., Detalle, V., Holl, Y., 2011. Laser-induced breakdown spectroscopy for polymer identification. Anal. Bioanal. Chem. 400 (10), 3331–3340. https://doi.org/10.1007/s00216-011-4898-2.

Hamzah, M., Khenfouch, M., Rjeb, A., Sayouri, S., Houssaini, D.S., Darhouri, M., Srinivasu, V.V., 2018. Surface chemistry changes and microstructure evaluation of low density nanocluster polyethylene under natural weathering: a spectroscopic investigation. J. Phys.: Conf. Ser. 984, 12010. https://doi.org/10.1088/1742-6596/984/1/012010.

He, K., Zhang, X., Ren, S., Sun, J., 2016. Deep residual learning for image recognition. In: Proceedings of the IEEE Conference on Computer Vision and Pattern Recognition, pp. 770–778.

Jambeck, J.R., Geyer, R., Wilcox, C., Siegler, T.R., Perryman, M., Andrady, A., Narayan, R., Law, K.L., 2015. Plastic waste inputs from land into the ocean. Science 347 (6223), 768–771.

V. Jung, M.R., Horgen, F.D., Orski, S.V, Rodriguez, C., Beers, K.L., Balazs, G.H., Jones, T. T., Work, T.M., Brignac, K.C., Royer, S.-J., Hyrenbach, K.D., Jensen, B.A., Lynch, J. M, 2018. Validation of ATR FT-IR to identify polymers of plastic marine debris, including those ingested by marine organisms Mar. Pollut. Bull. 127, 704–716. https://doi.org/10.1016/j.marpolbul.2017.12.061.

Junjuri, R., Gundawar, M.K., 2019. Femtosecond laser-induced breakdown spectroscopy studies for the identification of plastics. J. Anal. At. Spectrom. 34 (8), 1683–1692. https://doi.org/10.1039/C9JA00102F.

Junjuri, R., Gundawar, M.K., 2020. A low-cost LIBS detection system combined with chemometrics for rapid identification of plastic waste. Waste Manag. 117, 48–57. https://doi.org/10.1016/j.wasman.2020.07.046.

Junjuri, R., Zhang, C., Barman, I., Gundawar, M.K., 2019. Identification of post-consumer plastics using laser-induced breakdown spectroscopy. Polym. Test. 76, 101–108. https://doi.org/10.1016/j.polymertesting.2019.03.012.

Karaca, A.C., Ertürk, A., Güllü, M.K., Elmas, M., Ertürk, S., 2013. Automatic waste sorting using shortwave infrared hyperspectral imaging system. In: 2013 5th Workshop on Hyperspectral Image and Signal Processing: Evolution in Remote Sensing (WHISPERS), pp. 1–4. https://doi.org/10.1109/WHISPERS.2013.8080744.

Kiranyaz, S., Avci, O., Abdeljaber, O., Ince, T., Gabbouj, M., Inman, D.J., 2021. 1D convolutional neural networks and applications: a survey. Mech. Syst. Signal Process. 151, 107398 https://doi.org/10.1016/j.ymssp.2020.107398.

La Mantia, F.P., Morreale, M., Botta, L., Mistretta, M.C., Ceraulo, M., Scaffaro, R, 2017. Degradation of polymer blends: a brief review. Polym. Degrad. Stab. 145, 79–92. https://doi.org/10.1016/j.polymdegradstab.2017.07.011.

LeCun, Y., Bengio, Y., Hinton, G., 2015. Deep learning. Nature 521 (7553), 436–444. https://doi.org/10.1038/nature14539.

Liu, K., Tian, D., Wang, H., Yang, G., 2019. Rapid classification of plastics by laser-induced breakdown spectroscopy (LIBS) coupled with partial least squares discrimination analysis based on variable importance (VI-PLS-DA). Anal. Methods 11 (9), 1174–1179. https://doi.org/10.1039/C8AY02755B.

Liu, R., Lehman, J., Molino, P., Such, F. P., Frank, E., Sergeev, A., & Yosinski, J. (2018). An intriguing failing of convolutional neural networks and the coordconv solution. *ArXiv Preprint ArXiv:1807.03247*.

Locock, K., Deane, J., Kosior, E., Prabaharan, H., Skidmore, M., Hutt, O.E., 2017. The Recycled Plastics Market: Global Analysis and Trends. CSIRO, Australia.

Munno, K., De Frond, H., O'Donnell, B., Rochman, C.M., 2020. Increasing the accessibility for characterizing microplastics: introducing new application-based and spectral libraries of plastic particles (SLoPP and SLoPP-E). Anal. Chem. 92 (3), 2443–2451. https://doi.org/10.1021/acs.analchem.9b03626.

Murthy, V.N., Singh, V., Chen, T., Manmatha, R., Comaniciu, D., 2016. Deep decision network for multi-class image classification. In: IEEE Conference on Computer Vision and Pattern Recognition (CVPR), pp. 2240–2248. https://doi.org/10.1109/CVPR.2016.246.

Musu, W., Tsuchida, A., Kawazumi, H., Oka, N., 2019. Application of PCA-SVM and ANN techniques for plastic identification by Raman spectroscopy. In: 2019 1st International Conference on Cybernetics and Intelligent System (ICORIS), 1, pp. 114–118. https://doi.org/10.1109/ICORIS.2019.8874880.

Neo, E.R.K., Yeo, Z., Low, J.S.C., Goodship, V., Debattista, K., 2022. A review on chemometric techniques with infrared, Raman and laser-induced breakdown spectroscopy for sorting plastic waste in the recycling industry. Resour. Conserv. Recycl. 180, 106217 https://doi.org/10.1016/j.resconrec.2022.106217.

Ng, W., Minasny, B., McBratney, A., 2020. Convolutional neural network for soil microplastic contamination screening using infrared spectroscopy. Sci. Total Environ. 702, 134723 https://doi.org/10.1016/j.scitotenv.2019.134723.

Ng, W., Minasny, B., Montazerolghaem, M., Padarian, J., Ferguson, R., Bailey, S., McBratney, A.B., 2019. Convolutional neural network for simultaneous prediction of several soil properties using visible/near-infrared, mid-infrared, and their combined spectra. Geoderma 352, 251–267. https://doi.org/10.1016/j.geoderma.2019.06.016.

Ocean Insight. (n.d.). SpeedSorterTM LIBS sorting sensor. Retrieved August 10, 2020, from https://www.oceaninsight.com/products/systems/sorting-systems/speedsorter/.

OECD. (2018). Improving plastics management: trends, policy responses, and the role of international co-operation and trade.

Peng, X., Xu, B., Xu, Z., Yan, X., Zhang, N., Qin, Y., Ma, Q., Li, J., Zhao, N., Zhang, Q., 2021. Accuracy improvement in plastics classification by laser-induced breakdown spectroscopy based on a residual network. Opt. Express 29 (21), 33269–33280. https://doi.org/10.1364/OE.438331.

PEW Charitable Trusts;, & SYSTEMIQ. (2020). Breaking the plastic wave. https://www.pewtrusts.org/-/media/assets/2020/07/breakingtheplasticwave_report.pdf.

Pieszczek, L., Daszykowski, M., 2019. Improvement of recyclable plastic waste detection – a novel strategy for the construction of rigorous classifiers based on the hyperspectral images. Chemometr. Intellig. Lab. Syst. 187, 28–40. https://doi.org/10.1016/j.chemolab.2019.02.009.

Plastics Europe. (2022). Plastics - the facts 2021. https://plasticseurope.org/knowledge-hub/plastics-the-facts-2021/.

Rani, M., Marchesi, C., Federici, S., Rovelli, G., Alessandri, I., Vassalini, I., Ducoli, S., Borgese, L., Zacco, A., Bilo, F., Bontempi, E., Depero, L.E., 2019. Miniaturized near-infrared (MicroNIR) spectrometer in plastic waste sorting. Materials 12 (17). https://doi.org/10.3390/ma12172740.

Riese, F.M., Keller, S., 2019. Soil texture classification with 1D convolutional neural networks based on hyperspectral data. In: *ISPRS Ann. Photogramm. Remote Sens. Spatial Inf. Sci., IV-2/W5*, pp. 615–621. https://doi.org/10.5194/isprs-annals-IV-2-W5-615-2019.

Ritchie, H. (2018). Plastic pollution. Our world in data. https://ourworldindata.org/plastic-pollution.

Roh, S.-B., Oh, S.-K., Park, E.-K., Choi, W.Z., 2017. Identification of black plastics realized with the aid of Raman spectroscopy and fuzzy radial basis function neural networks classifier. J. Mater. Cycles Waste Manag. 19 (3), 1093–1105. https://doi.org/10.1007/s10163-017-0620-6.

Roh, S.-B., Park, S.-B., Oh, S.-K., Park, E.-K., Choi, W.Z., 2018. Development of intelligent sorting system realized with the aid of laser-induced breakdown spectroscopy and hybrid preprocessing algorithm-based radial basis function neural networks for recycling black plastic wastes. J. Mater. Cycles Waste Manag. 20 (4), 1934–1949. https://doi.org/10.1007/s10163-018-0701-1.

Saeki, K., Tanabe, K., Matsumoto, T., Uesaka, H., Amano, T., Funatsu, K., 2003. Prediction of polyethylene density by near-infrared spectroscopy combined with neural network analysis. J. Comput. Chem. Jpn. 2, 33–40. https://doi.org/10.2477/jccj.2.33.

Said, M., Amr, M., Sabry, Y., Khalil, D., Wahba, A., 2020. Plastic sorting based on MEMS FTIR spectral chemometrics sensing. Proc. SPIE 11354. https://doi.org/10.1117/12.2555876.

Sato, H., Shimoyama, M., Kamiya, T., Amari, T., Šašic, S., Ninomiya, T., Siesler, H.W., Ozaki, Y., 2002. Raman spectra of high-density, low-density, and linear low-density polyethylene pellets and prediction of their physical properties by multivariate data analysis. J. Appl. Polym. Sci. 86 (2), 443–448. https://doi.org/10.1002/app.10999.

Schyns, Z.O.G., Shaver, M.P., 2020. Mechanical recycling of packaging plastics: a review. Macromol. Rapid Commun., 2000415

Serranti, S, Cucuzza, P., Bonifazi, G., 2020. Hyperspectral imaging for VIS-SWIR classification of post-consumer plastic packaging products by polymer and color. Proc. SPIE 11525. https://doi.org/10.1117/12.2580504.

Serranti, Silvia, Gargiulo, A., Bonifazi, G., 2012. Hyperspectral imaging for process and quality control in recycling plants of polyolefin flakes. J. Near Infrared Spectrosc. 20 (5), 573–581. https://doi.org/10.1255/jnirs.1016.

Serranti, Silvia, Luciani, V., Bonifazi, G., Hu, B., Rem, P.C., 2015. An innovative recycling process to obtain pure polyethylene and polypropylene from household waste. Waste Manag. 35, 12–20. https://doi.org/10.1016/j.wasman.2014.10.017.

Specim. (2020). Specim FX50. https://www.specim.fi/wp-content/uploads/2020/03/Specim-FX50-Technical-Datasheet-02.pdf.

Stiebel, T., Bosling, M., Steffens, A., Pretz, T., Merhof, D., 2018. An inspection system for multi-label polymer classification. In: 2018 IEEE 23rd International Conference on Emerging Technologies and Factory Automation (ETFA), 1, pp. 623–630. https://doi.org/10.1109/ETFA.2018.8502474.

Szegedy, C., Liu, W., Jia, Y., Sermanet, P., Reed, S., Anguelov, D., Erhan, D., Vanhoucke, V., Rabinovich, A., 2015. Going deeper with convolutions. In: Proceedings of the IEEE Conference on Computer Vision and Pattern Recognition, pp. 1–9.

Ulrici, A., Serranti, S., Ferrari, C., Cesare, D., Foca, G., Bonifazi, G., 2013. Efficient chemometric strategies for PET–PLA discrimination in recycling plants using hyperspectral imaging. Chemometr. Intellig. Lab. Syst. 122, 31–39. https://doi.org/10.1016/j.chemolab.2013.01.001.

Vahid Dastjerdi, M., Mousavi, S.J., Soltanolkotabi, M., Nezarati Zadeh, A., 2018. Identification and sorting of PVC polymer in recycling process by laser-induced breakdown spectroscopy (LIBS) combined with support vector machine (SVM) model. Iran. J. Sci. Technol., Trans. A: Sci. 42 (2), 959–965. https://doi.org/10.1007/s40995-016-0084-x.

Wang, Y., Li, M., Ji, R., Wang, M., Zheng, L., 2020. Comparison of soil total nitrogen content prediction models based on Vis-NIR spectroscopy. Sensors 20 (24). https://doi.org/10.3390/s20247078.

Wienke, D., van den Broek, W., Melssen, W., Buydens, L., Feldhoff, R., Kantimm, T., Huth-Fehre, T., Quick, L., Winter, F., Cammann, K., 1995. Comparison of an adaptive resonance theory based neural network (ART-2a) against other classifiers for rapid sorting of post consumer plastics by remote near-infrared spectroscopic sensing using an InGaAs diode array. Anal. Chim. Acta 317 (1), 1–16. https://doi.org/10.1016/0003-2670(95)00406-8.

Wu, X., Li, J., Yao, L., Xu, Z., 2020. Auto-sorting commonly recovered plastics from waste household appliances and electronics using near-infrared spectroscopy. J. Clean. Prod. 246, 118732 https://doi.org/10.1016/j.jclepro.2019.118732.

Yan, X., Peng, X., Qin, Y., Xu, Z., Xu, B., Li, C., Zhao, N., Li, J., Ma, Q., Zhang, Q., 2021. Classification of plastics using laser-induced breakdown spectroscopy combined with principal component analysis and K nearest neighbor algorithm. Results Opt. 4, 100093 https://doi.org/10.1016/j.rio.2021.100093.

Yang, Y., Zhang, X., Yin, J., Yu, X., 2020. Rapid and nondestructive on-site classification method for consumer-grade plastics based on portable NIR spectrometer and machine learning. J. Spectrosc. 2020, 6631234 https://doi.org/10.1155/2020/6631234.

Yu, Y., Guo, L.B., Hao, Z.Q., Li, X.Y., Shen, M., Zeng, Q.D., Li, K.H., Zeng, X.Y., Lu, Y.F., Ren, Z., 2014. Accuracy improvement on polymer identification using laser-induced breakdown spectroscopy with adjusting spectral weightings. Opt. Express 22 (4), 3895–3901. https://doi.org/10.1364/OE.22.003895.

Zhang, X., Lin, T., Xu, J., Luo, X., Ying, Y., 2019. DeepSpectra: an end-to-end deep learning approach for quantitative spectral analysis. Anal. Chim. Acta 1058, 48–57. https://doi.org/10.1016/j.aca.2019.01.002.

Zheng, Q., Fang, W., Fan, J., 2020. Determination of antioxidant irganox 1010 in polypropylene by infrared spectrometry. IOP Conf. Ser.: Earth Environ. Sci. 514 (5), 52046. https://doi.org/10.1088/1755-1315/514/5/052046.

Zhu, S., Chen, H., Wang, M., Guo, X., Lei, Y., Jin, G., 2019. Plastic solid waste identification system based on near infrared spectroscopy in combination with support vector machine. Adv. Ind. Eng. Polym. Res. 2 (2), 77–81. https://doi.org/10.1016/j.aiepr.2019.04.001.

Zvekic, M., Richards, L.C., Tong, C.C., Krogh, E.T., 2022. Characterizing photochemical ageing processes of microplastic materials using multivariate analysis of infrared spectra. Environ. Sci.: Process. Impacts 24 (1), 52–61. https://doi.org/10.1039/D1EM00392E.